

Causes and mechanisms of the 2011–2012 El Hierro (Canary Islands) submarine eruption

Joan Martí,¹ Virginie Pinel,² Carmen López,³ Adelina Geyer,¹ Rafael Abella,³ Marta Tárraga,¹ María José Blanco,⁴ Antonio Castro,⁵ and Carmen Rodríguez⁵

Received 30 July 2012; revised 7 November 2012; accepted 7 January 2013; published 12 March 2013.

[1] El Hierro eruption started on 10 October 2011 after an unrest episode that initiated on 17 July 2011. This is the first eruption in the Canary Islands that has been tracked in real time. Although being submarine and not directly observable, the data recorded allowed its reconstruction and to identify its causes and mechanisms. Seismicity, surface deformation, and petrological data indicate that a batch of basanitic magma coming from a reservoir located at a depth of about 25 km below the El Hierro Island was emplaced at shallower depth creating a new reservoir about 10–12 km above, where magma evolved until the initiation of the eruption. The characteristics of seismicity and surface deformation suggest that the necessary space to accumulate magma at this shallower position, which coincides with the crust/mantle boundary beneath El Hierro, was created in about 2 months by elastic deformation and magma-driven fracturing of the crust. After this first intrusion episode, part of the magma started to migrate laterally toward the SE for nearly 20 km, always keeping the same depth and following a path apparently controlled by stress barriers created by tectonic and rheological contrasts in the upper lithosphere. This lateral migration of magma ended with a submarine eruption at about 5 km offshore from the southern corner of El Hierro Island. The total seismic energy released during the unrest episode was of 8.1×10^{11} J, and the total uplift previous to the onset of the eruption was of 40 mm. Combining geological, geophysical, and petrological data and numerical modeling, we propose a volcanological model of the causes and mechanisms of El Hierro eruption that shows how the stress distribution in the crust beneath El Hierro, which was influenced by rheological contrasts, tectonic stresses, and gravitational loading, controlled the movement and eruption of magma. We also discuss the implications of this model in terms of eruption forecast in the Canary Islands.

Citation: Martí, J., V. Pinel, C. López, A. Geyer, R. Abella, M. Tárraga, M. J. Blanco, A. Castro, and C. Rodríguez (2013), Causes and mechanisms of the 2011–2012 El Hierro (Canary Islands) submarine eruption, *J. Geophys. Res. Solid Earth*, 118, 823–839, doi:10.1002/jgrb.50087.

1. Introduction

[2] The Canary Islands is a populated ultraperipheral Spanish region and one of the most popular touristic destinations in Europe (Figure 1). The Canary Islands is one of the major volcanic ocean island groups of the world, where all islands, except for La Gomera, show Holocene volcanic

activity. Historical volcanism (last 600 years) has been reported on the islands of La Palma (1585, 1646, 1677, 1712, 1949, 1971), Tenerife (1704, 1706, 1798, 1909), and Lanzarote (1730–1736, 1824) and has been mainly characterized by short-lived (from few weeks to few months), Hawaiian, Strombolian, to violent Strombolian eruptions of mafic magmas, which have generated scoria cones of different sizes and lava flows of various extent [Romero, 1991]. All eruptions that occurred in the historical period, from 1402 until present, have typically been separated a few tens of years, but occasionally, some have occurred in a very narrow period of time (e.g., Arafo (1704), Fasnía (1705), Siete Fuentes (1705) in Tenerife) or have lasted for several years (Timanfaya eruption in Lanzarote, 1730–1736).

[3] Historical chronicles document how most of the Canarian historical eruptions were preceded by seismic unrest episodes of different durations, which were perceived by the local population [Romero, 1991]. Also, several seismic swarms not directly related to volcanic eruptions occurred in historical times [Romero, 1991]. Unfortunately, systematic monitoring in the Canary Islands did not start until the early

All supporting information may be found in the online version of this article.

¹Group of Volcanology (GVB-CSIC), SIMGEO (UB-CSIC), Institute of Earth Sciences Jaume Almera, Barcelona, Spain.

²ISTerre-CNRS-IRD-Université de Savoie, Le Bourget du Lac, France.

³Observatorio Geofísico Central, Instituto Geográfico Nacional (IGN), Madrid, Spain.

⁴Centro Geofísico de Canarias, IGN, Santa Cruz de Tenerife, Spain.

⁵Departamento de Geología, Universidad de Huelva, Huelva, Spain.

Corresponding author: J. Martí, Group of Volcanology (GVB-CSIC), SIMGEO (UB-CSIC), Institute of Earth Sciences Jaume Almera, Lluís Solé Sabarís s/n, 08028 Barcelona, Spain. (joan.marti@ictja.csic.es)

©2013. American Geophysical Union. All Rights Reserved.
2169-9313/13/10.1002/jgrb.50087

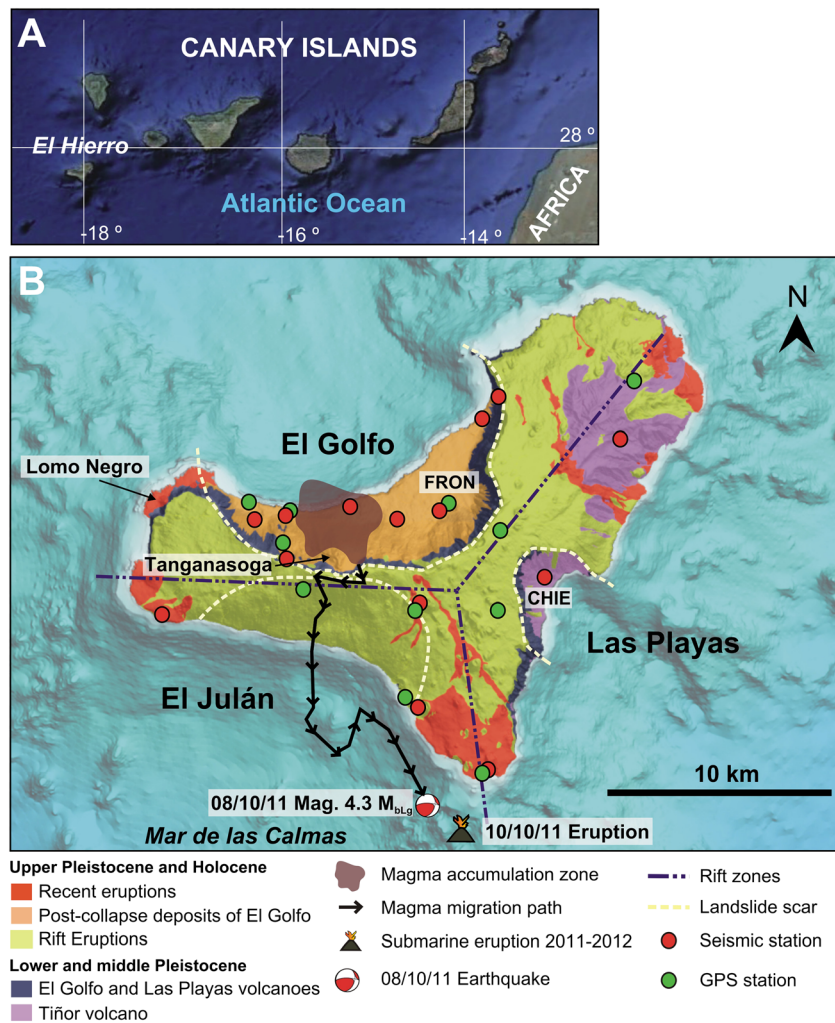


Figure 1. (a) Location map of the Canary Islands. (b) Simplified geologic map of El Hierro [from *Ancochea et al.*, 2004] showing the main morphological and structural features, and the epicentral migration of seismicity with time (see Supporting Information). Location and focal mechanism of the earthquake preceding the onset of the eruption, and location of the vent are also shown. Dark blue dashed lines are trace of the rift zones. White dashed lines are traces of landslides scars. CHIE, Seismic station; FRON, Frontera GPS station.

1980s, when the Spanish National Geographic Institute (IGN) installed a seismic network as part of the national network for seismic monitoring, so there are no monitoring records of the most recent eruptions, and everything we know about previous volcanism is based on historical chronicles and volcanological studies of past eruptions [Romero, 1991; Sobrado et al., 2011]. The IGN monitoring network was significantly improved and redesigned for volcano monitoring following an unrest episode that occurred in Tenerife in 2004 [Martí et al., 2009].

[4] The El Hierro eruption started on 10 October 2011 on the southern submarine flank of the island, at about a 5 km distance from the town of La Restinga and at a depth of 900 m below sea level (Figure 1). The eruption was preceded by nearly 3 months of unrest in which more than 11,000 seismic events, a total of 4 cm in surface deformation, and anomalous gas emissions were recorded by the IGN monitoring network (available at www.ign.es) [López et al., 2012]. The eruptive activity decreased drastically on 27 February 2012, and since then to the time of this writing (14 June

2012), only residual gas emissions have been registered from the main vent site. This eruption marked the end of a 40 years period of quiescence in the Canary Islands following the 1971 eruption of Teneguia in La Palma.

[5] The El Hierro eruption is the first one that has been fully monitored in real time since the beginning of unrest, so the amount of information available is significant. Despite being a submarine eruption without continuous observation of its evolution in terms of physical volcanology, on different days, the appearance of fragments of lavas and pyroclasts floating on the sea surface has permitted the obtainment of a good record of the volcanic products for petrological studies [Sigmarsson et al., 2012; Martí et al., accepted]. Also, the acquisition of bathymetric data by the Spanish Oceanographic Institute and the Spanish Research Council at different days during and after the eruption and their comparison with data obtained before the eruption has permitted to estimate the volume of emitted products and eruption rates.

[6] Combining all available data with mathematical modeling, we elaborate a volcanological model on the causes and

mechanisms of this eruption and discuss it in terms of eruption forecasts for the Canary Islands. We analyze the temporal evolution of geophysical and geochemical indicators during the unrest and eruptive episodes and use all this information to build a model that explains how magma movement progressed during the whole period. We then use this model to discuss the causes for magma movement and the mechanisms that controlled eruption on the Earth's surface. Finally, we compare this with previous information on historical eruptions in the Canary Islands, in order to deduce any possible guideline to interpret the reawakening of volcanism and to forecast future eruptions in this region.

2. Geological Setting

[7] The Canary Islands is a roughly linear 500 km long chain grown on the passive margin of the African Plate within the eastern Central Atlantic Ocean (Figure 1). The Canarian archipelago is the result of a long volcanic and tectonic activity that started at around 60 Ma ago [Robertson and Stillman, 1979; Le Bas *et al.*, 1986; Araña and Ortiz, 1991; Marinoni and Pasquarè, 1994]. Several contrasting models have been proposed to explain the origin of the Canary Islands. These include a hot spot origin [Schmincke, 1982; Hoernle and Schmincke, 1993; Carracedo *et al.*, 1998], a propagating fracture from the Atlas [Le Pichon and Fox, 1971; Anguita and Hernan, 1975], and mantle decompression melting associated with uplift of tectonic blocks [Araña and Ortiz, 1991]. However, each of the latter hypotheses presented some inconsistencies with the local and regional geology. A unifying model has been proposed by Anguita and Hernan [2000] who consider the existence of a residual of a fossil plume under North Africa, the Canary Islands, and western and central Europe defined through seismic tomography [Hoernle *et al.*, 1995]. Thus, volcanism is assumed to occur there, where an efficient fracture system allows the magma to ascent [Anguita and Hernan, 2000], i.e., the central European rift system, the volcanic provinces of the westernmost 60 Mediterranean (Balearic and Alboran basins), Iberia, the Canary Islands, and Cape Verdes [Hoernle *et al.*, 1995].

[8] Although all islands, except for La Gomera, show Holocene volcanic activity, historical volcanism has been restricted to La Palma, Lanzarote, and Tenerife Islands. In all cases, historical eruptive activity has been related to mafic magmas ranging in intensity from Hawaiian to violent Strombolian and has been the origin of scoria cones and lavas. Commonly, the historical eruptions have occurred on active rift zones along eruptive fissures occasionally generating alignments of cones. The duration of the eruptions ranges from a few weeks to a few months, except in the case of the Timanfaya eruption in 1730 that lasted 6 years. The total volume of extruded magma ranges from 0.01 to $>1.5 \text{ km}^3$ dense-rock equivalent (DRE), the latter being the case of Timanfaya. The eruption sequences that may be deduced from the successions of deposits differ from one eruption to another and reveal that eruptions do not follow a common pattern. In all cases, the resulting volcanic cones were constructed during single eruptive episodes (i.e., they must be referred to as monogenetic) commonly including several distinctive phases that do not show significant temporal separations between them.

[9] El Hierro is the youngest of the Canary Islands with the oldest subaerial rocks dated at 1.12 Ma and is situated at the southwestern corner of the archipelago [Guillou *et al.*, 1996]. El Hierro rises from 4000 m in depth to an altitude of about 1500 m above sea level and has an estimated volume of about 5500 km^3 [Carracedo *et al.*, 2001]. El Hierro corresponds to a shield structure formed by different volcanic edifices and includes three rift zones where recent volcanism is concentrated (Figure 1) [Guillou *et al.*, 1996; Carracedo *et al.*, 2001]. Other relevant morphological features are the collapse scars of El Golfo, Las Playas, and El Julian (Figure 1). The emerged parts of these rifts are defined by narrow and steep topographic ridges corresponding to aligned dike complexes with clusters of cinder cones. Pre-historical eruptions have been recognized on all three rifts of El Hierro [Guillou *et al.*, 1996; Carracedo *et al.*, 2001].

[10] Subaerial recent volcanism at El Hierro is monogenetic and has been mostly characterized by the eruption of mafic magmas ranging in composition from picrobasalts to basanites [Stroncik *et al.*, 2009], which have preferentially erupted along the rift zones forming cinder cones and lava flows. The erupted volume of magma in these eruptions typically ranges from 0.001 to 0.1 km^3 (DRE), these values being of the same order than most of the historical eruptions in the Canaries [Sobrado *et al.*, 2011]. One of the most important eruptive episodes of the last few thousand years of El Hierro corresponds to the Tanganasoga eruption (Figure 1). This eruption occurred inside the El Golfo depression, along an N-S-oriented fissure on which several cones and emission centers formed, giving rise to the construction of one of the largest volcanic edifices of the island by accumulation of ankaramitic lavas and pyroclastic deposits (Figure 1) [Carracedo *et al.*, 2001]. In addition to the subaerial volcanism, bathymetric studies [Gee *et al.*, 2001] have revealed that a significant number of well-preserved volcanic cones exist on the submarine flanks of the island, in particular on the continuation of the southern rift, which suggests that significant submarine volcanic activity has also occurred in recent times. Despite no existing historical chronicles on any of these eruptions, some authors [e.g., Hernandez-Pacheco, 1982] have suggested that the Lomo Negro eruption, located at the NW corner of the island (Figure 1) could have occurred in 1793, together with an important seismic swarm that was felt by El Hierro inhabitants and that was reported in their local chronicles.

3. Data

3.1. The Unrest Episode

[11] A detailed description of the procedures and monitoring data recorded during the unrest episode by IGN, the institution responsible for volcanic monitoring in Spain, can be found in López *et al.* [2012], and data are available at their website (www.ign.es) and in the supporting information, so in this section, we will only summarize the most relevant features of this episode.¹

[12] Before the volcanic reactivation of the El Hierro, volcano monitoring was basically done in two seismic stations that formed part of the Spanish seismic network for the whole Canarian archipelago and one Global Positioning System (GPS) station, FRON (Figure 1), belonging to the Canarian Regional Government, which was included in IGN

processing since summer 2010. As soon as the beginning of seismic unrest was detected in mid-July, the monitoring network was significantly improved with the deployment of eight new seismic stations, a seismic array, three accelerometers, nine new GPS stations, a permanent continuous gravimeter, four magnetic stations and five continuous Radon, CO₂, temperature and pressure stations (for location and details, see *López et al.*, [2012]). In addition, periodic surveys were conducted for microgravimetry and microgeodesy control, CO₂ measurements, and physical-chemical analysis of water springs all over the island.

[13] During nearly the first 2 months of unrest, seismic activity was concentrated at the north of the island in the offshore and inland sectors of El Golfo depression, the hypocenters being located at a depth of 10–15 km (Figure 2a and Table S1). Variation in epicentral location with time during this period defined a very irregular path going and turning back in all directions, always around the same area of 5 km² (Figure 1) (see supporting information). This episode of seismicity is interpreted as corresponding to the main pulse of magma intrusion and accumulation at a depth of 10–15 km [*López et al.*, 2012]. The characteristics of seismic events during this period clearly indicated the occurrence of volcano-tectonic events, probably caused by magma-driven fracturing of the host rock induced by the movement of magma and associated fluids [*López et al.*, 2012].

[14] During the second week of September, the location of epicenters marked a migration of seismicity toward the south, which may be interpreted as a lateral migration of magma (Figure 1). The depth of seismic events was kept nearly constant during this migration. The path defined by the location of seismic events described how magma turned around the eastern side of the Tanganasoga Volcano and then continued toward the south for more than 14 km (Figure 1), coinciding in location and orientation with one of the main linear high-gravity gradients found in the Canaries [*Carbó et al.*, 2003; *Montesinos et al.*, 2006]. The beginning of this lateral migration of magma coincided with a drastic acceleration on surface deformation (it reached 10 mm in a total of 40 mm of uplift in just 1 week) (Table S2). The accumulated seismic energy released [*López et al.*, 2012, Figure 4], which in this case is a measure of the resistance of the rock against the overpressure exerted by the magma [*Yokoyama*, 1988], exceeded the value of 1.0×10^{11} J on 27 September, thus indicating that the crust beneath El Hierro was highly strengthened. Since 27 September to the onset of the eruption on 10 October 2011, the IGN reported a new dramatic increase in the seismic activity, with more than 1100 new seismic events, of which over 90 were felt by the residents of the island, with a maximum intensity value of IV (EMS-98) [*López et al.*, 2012, Figure 4]. The total accumulated seismic energy released for the whole period of unrest was of 8.1×10^{11} J,

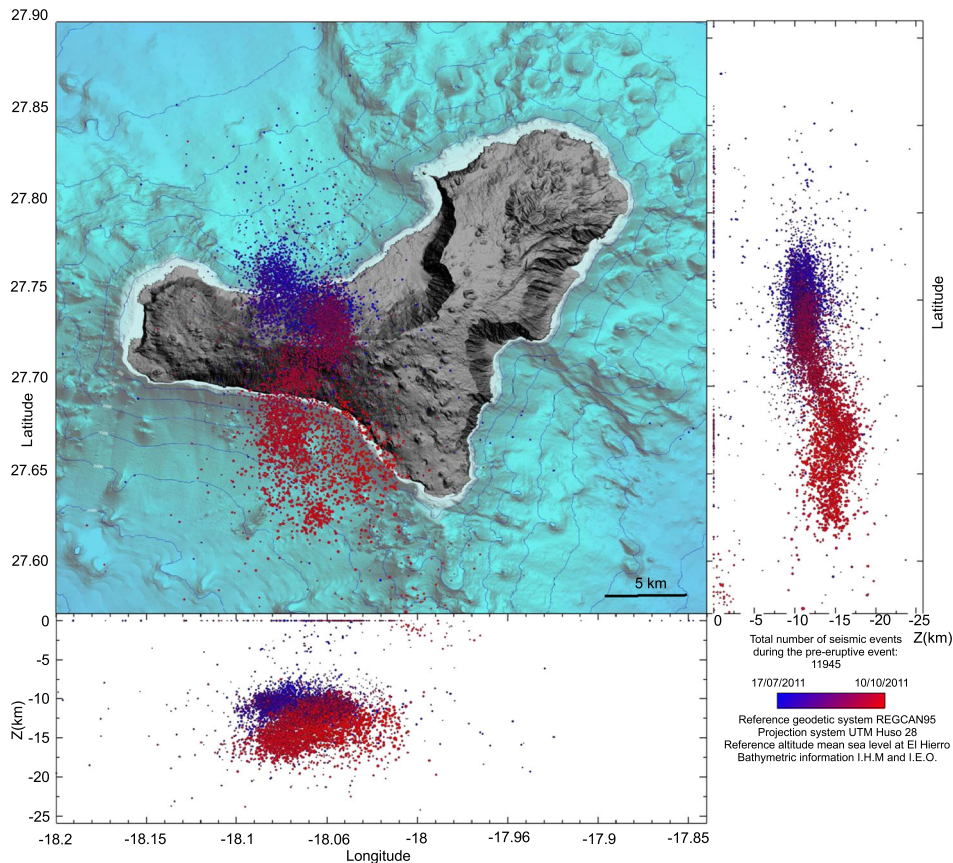


Figure 2. Epicentral and hypocentral locations of seismic events recorded from 17 July 2011 to 10 October 2011 (unrest episode). Data from IGN Seismic Catalogue (www.ign.es and supporting information).

which may be considered as a very high value if we compare it with other eruptions [Yokoyama, 1988]

[15] During the whole unrest period, very few deeper seismic events, which could suggest intrusion of deeper magma, were recorded. A seismic event of magnitude 4.3 M_{bLg} , located in the submerged part of the southern rift zone at a depth of 14 km, occurred 33 h before the onset of a submarine eruption at about 5 km from the SE corner of the island, at a depth of 900 m. After this seismic event, very few shallow earthquakes occurred before the culmination of the unrest episode. This suggests that magma used one of the main fissures of the southern rift system to rise in an aseismic manner to the surface at a velocity of 0.13 m s^{-1} .

3.2. The Eruption

[16] The first phases of the eruption were explosive and generated bombs and scoria fragments up to 30 cm in diameter that accumulated directly on the eruptive fissure, as reported by the first bathymetric survey carried out by the Spanish Institute of Oceanography (www.iao.es/hierro.htm) on 24–26 October 2011. Some of these pyroclastic fragments had low densities due to their high porosity and appeared floating at the sea surface. One of the particularities of the highly vesiculated volcanic bombs that appeared floating on 15 October 2011 was that they contained a pumice-like white core surrounded by a black scoriaceous carapace. The black component corresponded to a basanite (see Table 1), while the white one had a silicic composition [see Sigmarsson *et al.*, 2012]. The basanite is a typical composition of mafic magmas in El Hierro and in the Canaries in general. However, the felsic component is an uncommon product in Canarian volcanism. Some authors [Troll *et al.*, 2011; Perez-Torrado *et al.*, 2012] have suggested that it corresponds to xenoliths from pre-island sedimentary rocks that were picked up and heated by the ascending magma, causing them to partially melt and vesiculate. However, Sigmarsson *et al.* [2012], using trace element and isotopic compositions, concluded that an intrusion of gas-rich basanitic melt remobilized a stagnant trachytic melt that is present as a late differentiation in the volcanic edifice and that the trachyte incorporated and dissolved 10–15% of quartz sand that is present on the sea floor below El Hierro. This would explain the final rhyolitic composition of the white pumice without altering much the trace element composition of the original trachyte. The presence of sedimentary quartz involved in the generation of the white pumice of El Hierro, which Sigmarsson *et al.* [2012] attribute to turbidity sediments coming from the Saharan Platform, suggests that the assimilation and mingling processes gave rise to its formation initiated at the boundary between the pre-island basement and the bottom of the volcanic edifice, at a depth of 4000 m below sea level, and continued inside the eruption conduit. The fact that the first samples appeared a few days after the onset of the eruption constrains the time taken to form these anomalous white pumices. The rest of the samples that were collected and analyzed from the El Hierro eruption were all basanitic without any contamination of silicic material (Table 1) [Martí *et al.*, accepted], thus indicating that the formation of the white pumices was an anecdotic episode in this eruption.

[17] During the first 3 days of eruption, the eruptive focus migrated along the eruptive fissure to the north for about 3 km until reaching a depth of 300 m below sea level, at about 1800 m from the coast. At this point, its advance was

halted by an intersecting NE-SW regional normal fault (Figure 3). This favored the formation of a central eruptive conduit at the intersection between the two fracture planes and the construction of a volcanic edifice by the accumulation of pyroclastic material at the vent. This new volcanic edifice reached a total height of nearly 220 m, with the diameter of the base being more than 1000 m at the end of the eruption [Rivera *et al.*, 2013]. A lava flow was also emplaced from the base of the cone on a SW direction. A few parasitic vents also opened in later stages of the eruption around the main cone. The total amount of erupted volcanic material has been estimated from the extend and thickness of erupted products mapped by the marine surveys [Rivera *et al.*, 2013] and is of the order of 0.33 km^3 , thus giving an averaged eruption rate of $27 \text{ m}^3 \text{ s}^{-1}$. Assuming an average density of 2800 kg m^{-3} for the basanitic magma, the total amount of erupted magma is about 0.20 km^3 (DRE), which is in good agreement with the volumes of most of the historical eruptions in the Canaries [Sobrado *et al.*, 2011].

[18] During the first days of eruption, the associated seismicity was very weak, but almost 10 days after, strong tectonic and volcano-tectonic seismicity was concentrated at the north of the island and was located mostly at a depth of 20–25 km, and 10 days later, also at 10–15 km (Figures 4 and 5). Since the beginning, the eruption was accompanied by a continuous strong tremor located at the vent. The amplitude and stability of the volcanic tremor changed during the eruption, and occasionally, these variations were clearly associated with the occurrence of new seismic events in the north of the island, suggesting a direct connection between the site of the eruption and what was happening to more than 20 km north. In this sense, it is worth mentioning that the initiation in early November of intense seismicity located north at a depth of 20–25 km (Figure 5) coincided with the maximum expression of the eruption at the sea surface with the formation of giant bubbles and other visible manifestations (Figure 6). This also coincided with a significant increase of the tremor intensity (Figure 5).

[19] The syn-eruptive tectonic and volcano-tectonic seismicity observed at the north of the island first at a depth of 20–25 km and later at 10–15 km had slightly different orientations and epicentral locations than the seismicity recorded during the first weeks of unrest. We interpret most of the syn-eruptive seismicity as mainly caused by readjustments of the whole plumbing system following the decompression caused by the withdrawal of magma during the eruption, as it has occurred in other similar eruptions [Sigmondsson *et al.*, 2010; Tarasiewicz *et al.*, 2012]. Some of these new seismic events reached a magnitude of 4.6 and showed focal mechanisms compatible with N-S-oriented strike-slip faults.

[20] The petrology and geochemistry of the eruptive products indicate that magma composition was nearly constant during the whole process, only showing different equilibrium conditions of pyroxenes and olivines as corresponding to the storage and differentiation of magma at different depths (Table 1) [Martí *et al.*, accepted]. Disequilibrium observed in some olivine phenocrysts suggests a deeper provenance of the original magma. These petrological results are in good agreement with previous studies from the shallow plumbing system beneath El Hierro [Stronck *et al.*, 2009]. The temperature of the magma, estimated from pyroxene geothermometers and experimental petrology, showed a

Table 1. Whole Rock Compositions of the Studied Samples [from *Martí et al.*, accepted]

Sample	HB1	HB2	HB3	HB4	HB5	HB6	HB6	HB8	HB9	HB10	HB11
Date of emission	15 Oct 2011	31 Oct 2011	31 Oct 2011	31 Oct 2011	27 Nov 2011	5 Dec 2011	6 Dec 2011	5 Jan 2012	18 Jan 2012	21 Jan 2012	28 Jan 2012
SiO ₂ ^a	44.65	43.05	41.88	43.36	40.13	43.76	42.84	42.47	42.87	42.86	43.02
TiO ₂	4.64	4.83	4.73	4.59	4.87	4.68	4.74	4.7	4.77	4.78	4.78
Al ₂ O ₃	13.51	14.09	14.17	13.88	13.60	14.36	13.43	13.56	12.98	13.05	13.03
FeO _{tot} ^b	12.60	12.70	13.82	13.45	17.07	12.85	13.34	12.17	13.61	13.65	13.62
MgO	5.56	6.91	7.17	7.31	7.60	6.25	7.83	8.66	8.67	8.6	8.6
MnO	0.21	0.37	0.25	0.20	0.19	0.20	0.19	0.42	0.188	0.189	0.189
CaO	10.34	11.06	11.16	10.50	10.53	10.97	10.99	10.49	11.18	11.16	11.29
Na ₂ O	4.42	5.49	4.54	3.97	3.28	4.10	3.89	6.02	3.51	3.55	3.5
K ₂ O	1.14	1.71	1.57	1.55	1.49	1.59	1.46	1.56	1.39	1.4	1.4
P ₂ O ₅	0.88	n.d	n.d	0.92	0.78	0.95	0.84	n.d.	0.786	0.79	0.78
LOI	n.d. ^c	n.d	n.d	0.25	0.50	0.60	0.43	n.d.	0.74	0.61	0.65
Total	97.95	100.22	99.29	99.98	100.05	100.31	99.98	100.05	100.69	100.64	100.86
Mg# ^d	0.44	0.49	0.48	0.49	0.44	0.46	0.51	0.56	0.53	0.53	0.53
<i>Trace elements (ppm)</i>											
Li	9.22	8.07	8.92	8.20	6.04	9.18	8.56	7.27	7.78	8.34	7.30
Be	2.84	2.45	2.67	2.48	2.03	2.81	2.59	2.19	2.31	2.52	2.19
Sc	16.4	20.1	22.33	20.2	19.4	24.4	26.5	24.8	26.1	29.0	24.9
V	261	277	338	302	298	321	342	337	361	399	345
Cr	23.3	123	297	179	154	110	217	354	374	340	329
Co	37.1	82	45.3	40.2	61.9	80.3	81.7	46	49.3	53.6	46.5
Ni	41.2	74.9	96.9	80.2	89.9	59.6	114	141	154	166	142
Cu	71.2	68.3	77.2	69.8	72.9	80.0	87.6	86.9	93.8	103	103
Zn	151	140	146	134	130	154	154	130	136	151	129
Ga	25.9	23.5	25.7	23.5	20.5	26.2	25.7	22.5	23.6	25.8	22.2
Rb	37.6	34.3	35.5	30.7	26.9	35.6	34.5	27.9	28.6	31.4	26.8
Sr	1079	982	993	901	707	1117	1060	831	865	951	823
Y	36.7	33.2	37.1	33.1	24.6	37.9	35.9	30.8	31.9	34.8	30.3
Zr	291	286	402	367	261	410	381	379	371	371	371
Nb	78.1	72.1	72.7	66.7	50.4	80.3	73.9	61.3	63.8	68.4	59.9
Cs	0.64	0.61	0.48	0.41	0.47	0.50	0.49	0.37	0.40	0.44	0.38
Ba	414	376	426	391	331	426	396	359	379	403	355
La	66.9	59.7	62.6	57.3	50.2	65.3	59.8	49.3	52.1	55.2	48.4
Ce	135	121	132	120	104	138	126	104	110	118	103
Pr	16.3	14.7	16.6	15.1	12.9	17.4	15.9	13.2	14	14.9	13.03
Nd	64.9	59.2	69.4	62.6	52.8	71.3	66.1	56.1	59.4	63.7	55.05
Sm	12.5	11.6	13.9	12.4	11.0	14.3	13.5	11.5	12.0	13.1	11.2
Eu	3.83	3.57	4.32	3.99	3.37	4.40	4.13	3.68	3.87	4.16	3.62
Gd	10.2	9.49	11.6	10.6	9.09	11.9	11.2	9.74	10.3	11.1	9.62
Tb	1.37	1.28	1.47	1.36	1.21	1.51	1.44	1.28	1.33	1.42	1.26
Dy	6.99	6.57	8.39	7.58	6.36	8.39	7.78	6.98	7.32	8.01	6.88
Ho	1.25	1.18	1.41	1.27	1.11	1.38	1.31	1.18	1.24	1.33	1.16
Er	3.00	2.73	3.42	2.99	2.57	3.28	3.04	2.78	2.92	3.14	2.70
Tm	0.40	0.37	0.40	0.37	0.34	0.40	0.38	0.35	0.36	0.38	0.34
Yb	2.37	2.18	2.31	2.19	1.90	2.42	2.24	1.92	2.11	2.31	1.90
Lu	0.35	0.31	0.32	0.29	0.26	0.32	0.31	0.26	0.28	0.29	0.26
Hf	4.94	5.93	10.1	9.41	7.02	10.6	9.50	8.40	9.00	9.59	8.35
Ta	5.29	5.16	5.59	5.02	4.19	5.91	5.3	4.91	5.12	5.27	4.69
Pb	4.25	3.67	4.28	3.69	3.13	4.79	3.89	3.12	3.38	3.64	3.11
Th	6.68	5.811	5.69	5.14	5.07	5.97	5.60	4.50	4.76	5.06	4.43
U	1.91	1.578	1.60	1.41	1.35	1.70	1.556	1.25	1.35	1.44	1.24

^aMajor element analyses are given in wt% oxides.^bTotal Fe as FeO.^cn.d., Not determined.^dMg# = Molar MgO/MgO + FeO.

maximum variation of 126 °C, from 1206 °C to 1080 °C [Martí et al., accepted]. Although the general tendency of magma temperature is to decrease progressively from the first episodes to the last ones, in detail, it showed an irregular pattern that suggests the existence of various magma inputs into the shallow reservoir during the eruption. A similar pattern is shown by the degree of crystallinity, which ranges from 3% to more than 44% (Figure 7).

3.3. Variation of the Main Pre and Syn-eruptive Parameters With Time

[21] The patterns showed by seismicity and surface deformation suggest that the deeper reservoir (at ~20–25 km) started to decompress a few days after the initiation of the eruption, while the shallower reservoir (at ~10–15 km) remained overpressurized nearly until the end of November

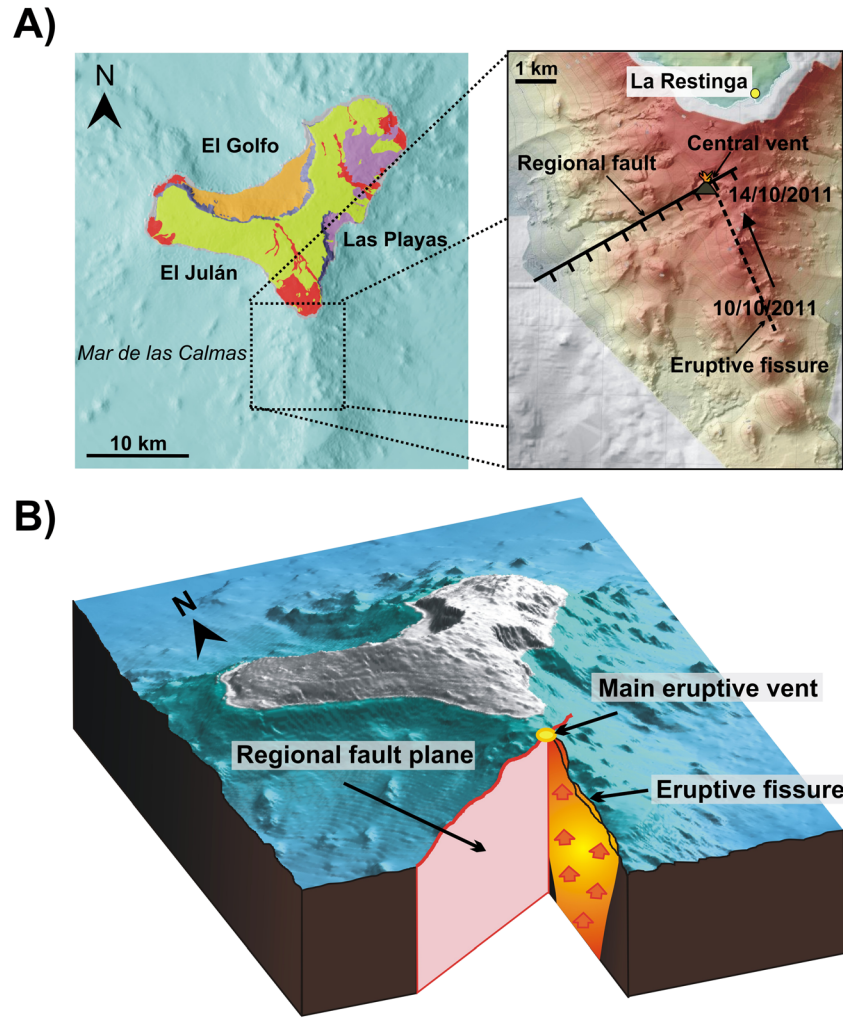


Figure 3. (a) DEM of the southern sector of El Hierro showing the trace of the eruptive fissure and its intersection with a NE-SW trending normal fault, where a central conduit and vent was formed. (b) Schematic explanation of the formation of a central conduit at the intersection of the two planes corresponding to the eruptive fissure and the normal fault, respectively.

2011. As a summary of the data acquired by the monitoring network and petrological study of the erupted products, we show in Figures 5 and 7 a comparison of the variation of the main physical and petrological parameters, respectively, with time (unrest plus eruption).

[22] One of the most interesting aspects of this eruption is the correlation of the main deformation episodes with the dynamics of each magma reservoir. In other words, we can see how each magma reservoir responded to stress changes triggered by decompression of the plumbing system, in a similar way to what occurred in the Eyjafjallajökull eruption in 2010 [Tarasewicz *et al.*, 2012]. Seismic anelastic deformation is a measure of irreversible deformation of the rock [Voight, 1968; Matsuki, 1991] and can be used to estimate the total volume necessary to place the magma in the crust corresponding to the fracturing that occurred when the elastic response had been exceeded. Figure 5a shows the temporal variation of anelastic strain as a measure of the response of the magma reservoir to the seismic deformation imposed by inflation (overpressurization) and deflation (decompression) episodes. To calculate it, we selected the corresponding IGN seismic catalogue data (www.ign.es, Table S1) for the seismic

series associated with El Hierro unrest and eruption, which accumulated more than 12,000 events in total. The scalar seismic moment, Mo (in N m), was estimated from the IGN calculated earthquake magnitude, mb , using the general equation of Chen and Chen [1989]:

$$\log Mo = 1.5 mb + 9.0 \text{ for } mb \leq 5.2. \quad (1)$$

[23] The cumulative seismic moment release for the earthquake sequence is as follows:

$$\sum Mo = \sum \mu A d, \quad (2)$$

where $\sum Mo$ is the fundamental parameter for the strength measurement of an earthquake caused by a fault slip, μ is the shear modulus of the host rock, d is the slip across the fault, and A is the fault surface area for each individual event.

[24] $\sum Mo$ represents a measure of the size of the irreversible anelastic deformation involved in the earthquake sequence during the magmatic process, and the accumulated

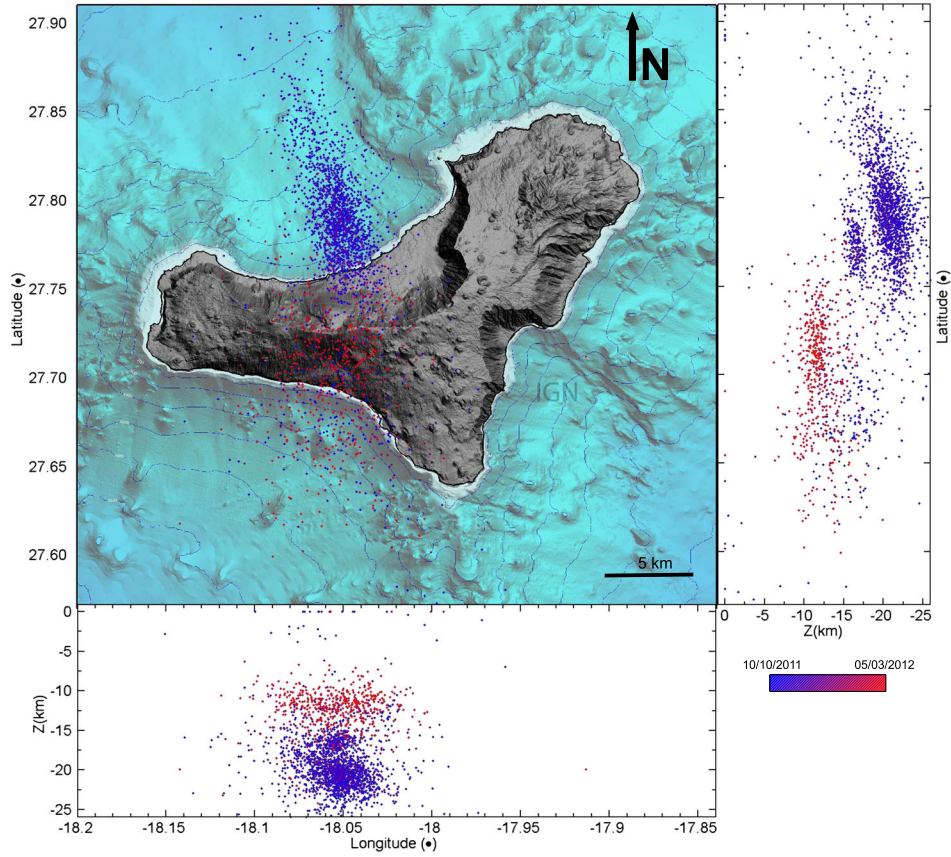


Figure 4. Epicentral and hypocentral locations of seismic events recorded from 10 October 2011 to 5 March 2012 (eruptive episode). Data from IGN Seismic Catalogue (www.ign.es and supporting information).

product, μAd , represents a source volume required to produce the anelastic deformation in a shear dislocation approximation [Aki and Richards, 1980, Hill *et al.*, 2003]. Taking a typical value of $\mu = 40$ GPa [Watts, 1994; Watts *et al.*, 1997] for the studied area, we computed the cumulative time variation of $\sum Mo/\mu$ (in m^3) for two selected groups of seismic data: earthquakes located at a depth less than 20 km (blue dots in Figure 5a) and earthquakes deeper than 20 km (red dots in Figure 5a). As can be observed on the depth-time variation curve at Figure 5a, all the preruptive events were located at a depth less than 20 km, and most of the syn-eruptive seismicity, including the most energetic events, correspond to depths greater than 20 km. This shows how, before the eruption, the anelastic deformation (associated with brittle fracturing) involved accommodation of magma in the shallow part of the plumbing system until it became stabilized with the beginning of the eruption (vertical black line (1) in Figure 5). This situation is maintained during the next 20 days after the eruption onset, until 30 October 2011 (vertical black line (2) in Figure 5) and included, approximately on 18 October 2011, the initiation of deeper seismicity at the north (see Figure 5b). From 30 October 2011 to 21 November 2011 (vertical black line (3) in Figure 5), deformation associated with the deeper reservoir is intensified, coinciding with major vertical deflation recorded by the GPS network (Figure 5c, Table S2). This suggests that the deepest reservoir started to collapse when it could not maintain its internal pressure. The difference in seismic anelastic strain volume between the two curves

shown in Figure 5a suggests that the deeper reservoir was larger than the shallower one.

[25] Figure 5c shows the north, east, up coordinate variations of the FRON permanent GPS station (Frontera, GRAFCAN network) (Figure 1) located at El Hierro using precise ephemerides in a local reference system. Even if the vertical component shows a higher scatter, it can be observed that the three components of the surface deformation experience a continuous increment until the onset of the eruption. Subsequent deflation can be recognized in the vertical component, coinciding with the increment of released seismic energy associated with the deeper reservoir, which remained stable thereafter.

[26] The Gutenberg-Richter b values [Gutenberg and Richter, 1954] are commonly used to discriminate between purely tectonic ($b < 1.5$) and volcano-tectonic events ($b > 1.5$), the latter being usually related to magma-driven fracturing of the host rocks induced by the movement of magma and associated fluids [Yokoyama, 1988]. In the case of El Hierro, to calculate the b value, we used the IGN earthquake catalogue for event magnitudes greater or equal to 2.0 M_{bLg} , giving a total of 2228 events. We calculated the b value using the maximum likelihood method. Results (Figure 5d) show that there was a significant variation of the Gutenberg-Richter b values with higher values at the beginning and a progressive decrease of b values as the process advanced and, in particular, once the eruption started.

[27] The onset of the eruption was accompanied by the appearance of a strong tremor signal in all seismic stations.

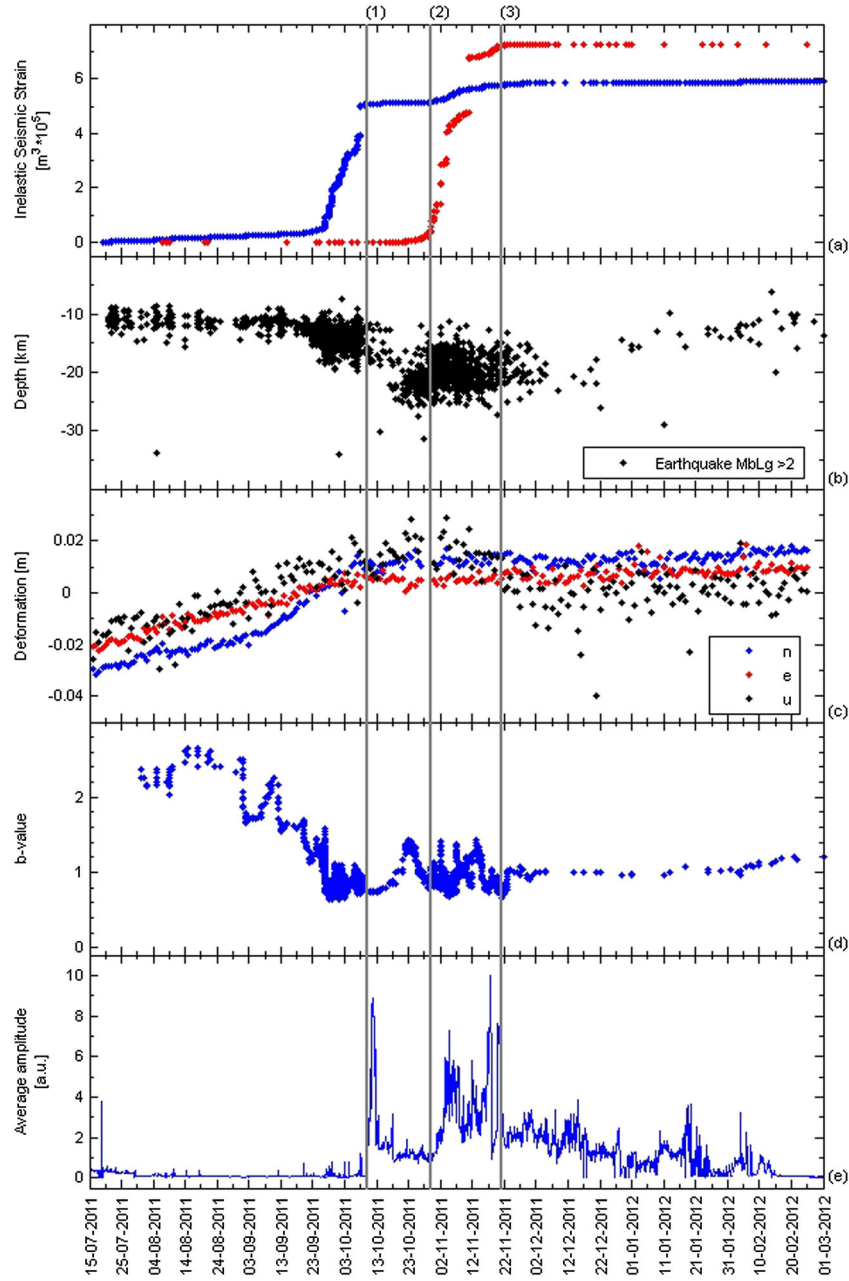


Figure 5. Diagram comparing the variation of the main geophysical parameters with time. (a) Anelastic seismic strain volume. (b) Depth of seismic events. (c) Surface deformation recorded at the FRON GPS station (see Figure 1 for location). (d) Gutenberg-Richter b value. (e) Average amplitude of the continuous seismic signal. Vertical black lines: (1) 10 October 2011 (eruption onset), (2) 27 October 2011, and (3) 21 November 2011. See text for more explanation.

The amplitude of this tremor experienced several changes during the eruption probably related to changes in pressure in the eruptive conduit and/or in the whole plumbing system [see Chouet, 1996; McNutt, 2005; Jellinek and Bercovici, 2011]. Figure 5e shows the time evolution of the 1 h average amplitude module (normalized) of the continuous seismic signal at CHIE station (Figure 1) filtered from 1 to 10 Hz. From the beginning of the eruption to 21 November 2011, the most energetic phase was recorded, coinciding with the stable behavior of the plumbing system during that period. A significant change in the amplitude of the continuous

seismic signal occurred on 21 November, probably associated with a significant collapse of the deeper part of plumbing systems following decompression, as mentioned before, and also due to important changes in the rheological properties of the erupting magma [Martí *et al.*, accepted]. This implied a progressive decrease of the intensity of the tremor, with this tendency being maintained until the end of the eruption.

[28] The petrological study of quenched magma samples has permitted to identify the main physicochemical time variations experienced by the erupted basanitic magma and

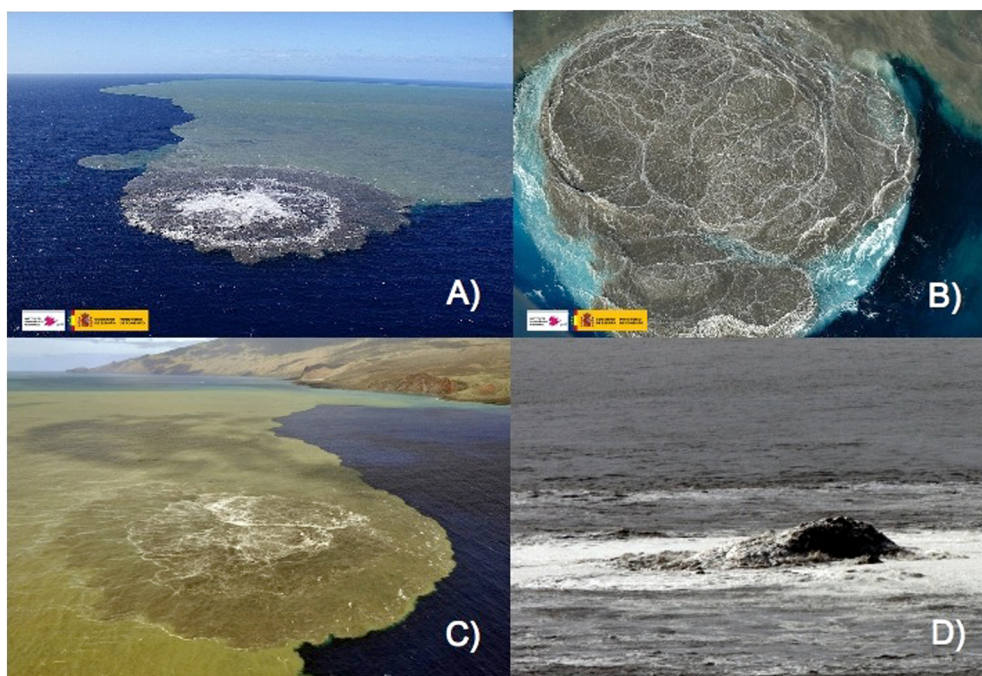


Figure 6. Photographs of the giant bubbles and other manifestations of the eruptive activity observed at the sea surface on the eruption vent in the early days of November, also coinciding with an increase of seismicity at the north of El Hierro and of the intensity of the tremor signal (see Figure 5). (a, b, c) Aerial views of the gigantic stain visible on the surface of Las Calmas Sea. Circular spot is approximately 1 km across. (d) Giant bubble formed on 4 November 2011. From IGN, EFE.

to distinguish between two main eruptive episodes (Figure 7) [Martí *et al.*, accepted]. Results indicate that magma which was erupted until late November 2011 (i.e., during the first eruptive episode) corresponded to a fractionated basanite ($\text{MgO} \approx 5 \text{ wt.}\%$) that evolved into more primitive compositions with time, thus suggesting extraction from a zoned magma chamber. The erupted magma was re-equilibrated at about 400 MPa, which corresponds to a depth of 12–15 km, coinciding with the location of the crust/mantle discontinuity beneath El Hierro [see Bosshard and MacFarlane, 1970; Watts, 1994]. Diffusion modeling data from olivine zoning [Martí *et al.*, accepted] suggest that the timescale for basanite fractionation in that shallow magma chamber was of the order of 3 months, which coincides with the duration of the unrest episode preceding the eruption. Abrupt changes in magma compositions and crystal content were observed at the end of November 2011, which started a second eruptive episode characterized by the emission of more primitive, less crystalline magma until the end of the eruption. The transition between the two eruptive episodes is correlated with an intrusion of fresh, more primitive magma into the shallow reservoir [Martí *et al.*, accepted].

4. Mechanistic Model

[29] As shown by seismicity and deformation data, the magma migrated, following a complex path, for 12 weeks before finding its way to reach the surface on 10 October 2011. This migration occurred at a depth around 15 km, which appears to correspond to the crust-mantle boundary. Magma migration was clearly influenced by the local stress field as evidenced by the way it turned around some volcanic

edifices in its migration to the SE and the fact that its final ascent occurred along a fault plane belonging to the southern rift zone system (Figures 1 and 3). However, at first order, we can consider that the magma first moved laterally toward the edifice center, then continued its way toward the other side to feed an eruption at some distance on the opposite flank. This behavior presents some similarities with the migration of the magmatic intrusion observed through InSAR measurement between August 1999 and April 2000 at Eyjafjallajökull volcano, where the feeding source was located on the northern flank of the volcano and magma migrated horizontally southward, producing inflation on the southern flank before a cessation of the unrest episode without any eruption [Pedersen and Sigmundsson, 2006].

[30] Magma migration through the Earth's brittle part of the lithosphere takes place by dike propagation, which implies a crustal fracture associated with magma transport [Lister and Kerr, 1991; Rubin, 1993; Petford *et al.*, 2000]. This phenomenon depends on the magma-driving overpressure, the physical properties of the magma (mainly its density and viscosity), and the surrounding crust (mainly its density, elastic properties, and tensile strength), as revealed by analytical studies [Lister, 1990; Lister and Kerr, 1991]. Magma migration is also clearly influenced by the local surrounding stress field as proven by analogical [Watanabe *et al.*, 1999] as well as numerical models [Pinel and Jaupart, 2004; Maccaferri *et al.*, 2011]. At El Hierro, the local stress field is influenced by the tectonic context as well as the lithospheric flexure induced by the edifice load. Here we will focus on the second aspect using an axisymmetric numerical model in order to quantify the stress field within the elastic part of the lithosphere but without taking into account

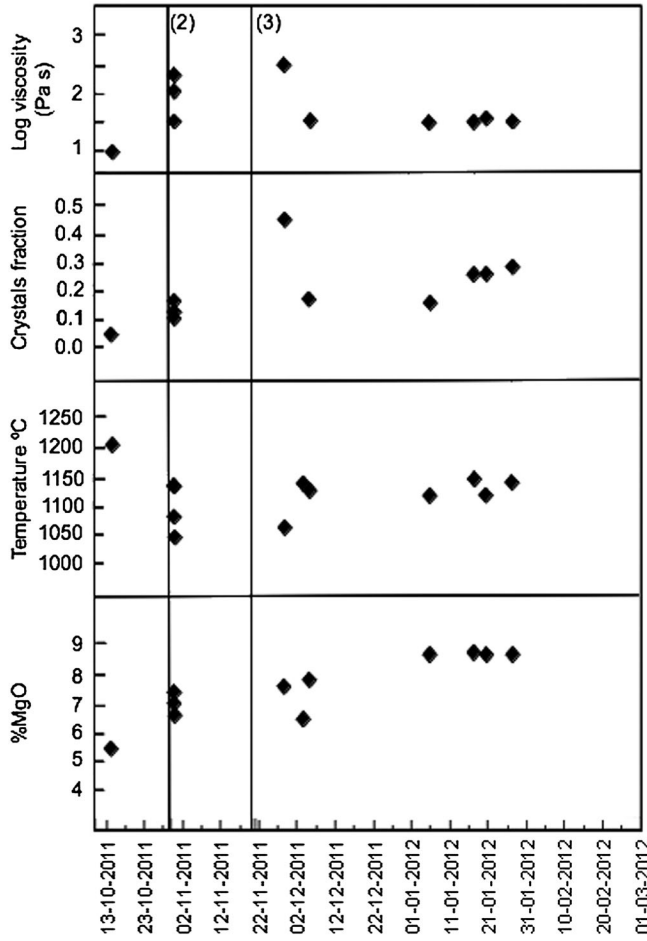


Figure 7. Diagram comparing the variation of the main petrological parameters (percentage of MgO, temperature, crystals content, viscosity) with time. Vertical black lines: same dates as in Figure 5.

volcano spreading. Stress and strain within the crust are numerically calculated, solving the equations for linear elasticity with the “Finite Element Method” (COMSOL software). A mesh of about 100,000 triangular units that is refined around the volcanic edifice is used. No displacement is allowed at the lateral boundary. A normal stress is applied at the upper boundary corresponding to the water and to the edifice loads (Figure 8). The whole medium is submitted to a gravity field. As El Hierro Island started its construction more than 1 Ma ago, the volcanic load is sufficiently long in duration to consider that a final relaxed state in isostatic equilibrium has been reached. It follows that the medium can be assimilated to an elastic lithosphere of given thickness lying over an inviscid fluid (the mantle). Due to the load, there is a flexure of the lithosphere [Watts, 1994], which gets partially immersed in the denser mantle. As a response to the lithospheric deflection, a buoyant restoring force acts at the bottom of the lithosphere, in a normal direction, opposing flexure. Such a boundary condition is classically used and sometimes called a “Winkler” foundation in the literature [Galgana *et al.*, 2011]. With the lithosphere being under sea level, part of this Winkler foundation, σ_B , is compensated by the water load, such that it can be expressed through the following relation:

$$\sigma_B = (\rho_m - \rho_w)gU_z, \quad (3)$$

where ρ_m and ρ_w are the mantle and the water density, respectively, and U_z is the vertical displacement at the base of the crust. The sign convention used is such that tensile stresses are negative. Numerical solutions were validated using analytical solutions for the displacement induced by the loading of a thick elastic plate lying over an inviscid medium provided by Pinel *et al.* [2007].

[31] As already explained by Mc Govern and Solomon [1993], lithospheric flexure due to the edifice load generates lateral stress characterized by a “dipole” pattern with horizontal extension in the lower lithosphere and compression in the upper lithosphere at the axis beneath the edifice. The amplitude of this effect decreases when going laterally away from the edifice. This effect acts together with the gravity field to produce the resulting stress field. Figure 9 shows the horizontal component $\sigma_{\theta\theta}$ of the stress field within the crust, when considering the parameters listed in Table 2. In the absence of edifice load at the surface (Figure 9a), the compression increases with depth due to the lithostatic load, whereas, when an edifice induces a lithospheric flexure (Figure 9b), this lithostatic load is, in the lower part of the crust, partly compensated by the tension due to the flexure, such that the compression is almost invariant with depth beneath the edifice axis. This effect decreases when going laterally away from the edifice.

[32] Figure 10 shows, on the same graph, the pressure profile (P_{magma}) within a basanitic magma (density 2800 kg m^{-3}) rising vertically from a slightly overpressurized source located at 25 km depth and the stress component $\sigma_{\theta\theta}$ profiles. With the $\sigma_{\theta\theta}$ being the normal stress acting on a vertical dyke propagating radially away or toward the edifice, the pressure difference, $P_{\text{magma}} - \sigma_{\theta\theta}$, can be directly related to the dyke opening, with the dyke being opened only when this term is positive. This figure illustrates three important points. Magma rising vertically through the mantle reaches the crustal bottom with a large overpressure, such that it would be expected to keep on propagating vertically. At the bottom crustal boundary, the horizontal stress $\sigma_{\theta\theta}$ increases when going away from the axis as a consequence of the flexural effect being maximal at the axis. It follows that a dyke intruding laterally at the crustal/mantle boundary should propagate toward the edifice center. This deduction is based on numerical calculation results showing that a surrounding decreasing stress favors lateral propagation versus vertical extension [Traversa *et al.*, 2010]. The third important point concerns the vertical gradient of the overpressure available for dyke opening $(P_{\text{magma}} - \sigma_{\theta\theta})/dz$. This gradient is negative, which is usually the case when the magma is denser than the surrounding crust. Here we consider a magma that is less dense than the surrounding crust. With no edifice load, the vertical gradient of the overpressure would be positive, ensuring the dyke ascent toward the surface. However, the edifice induces a flexure of the lithosphere and compression in the upper part of the crust, such that the vertical gradient of magma overpressure becomes negative. It means that when the dyke propagates vertically toward the surface, its progression is inhibited—the vertical extension of a dyke is limited. At some depth, when the rising magma pressure P_{magma} becomes lower than the surrounding stress field $\sigma_{\theta\theta}$, it prevents dyke opening. On Figure 10, we

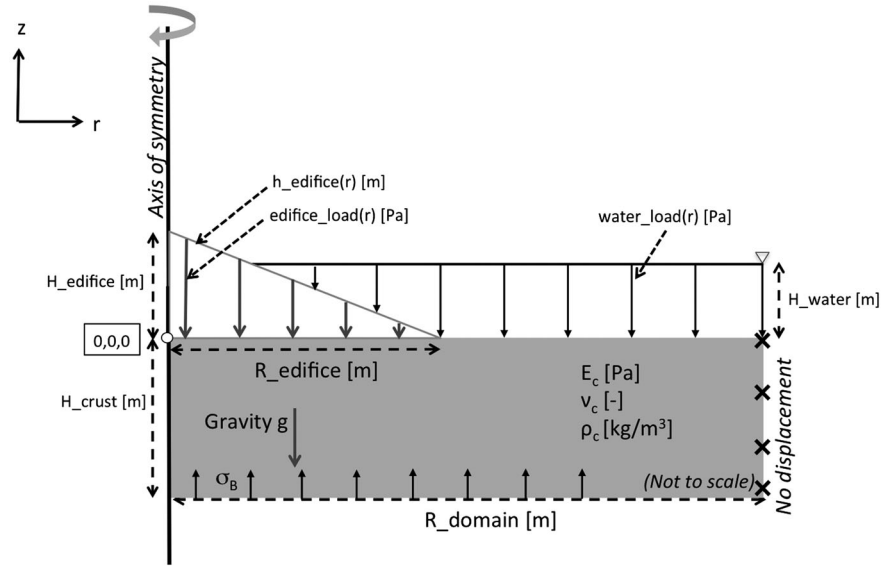


Figure 8. Model geometry and boundary conditions.

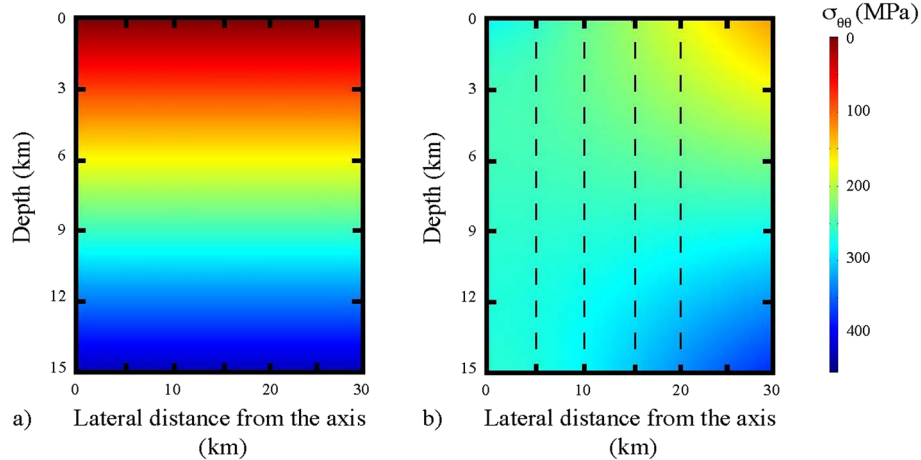


Figure 9. Amplitude of the horizontal stress component $\sigma_{\theta\theta}$ (acting normal to vertical dykes propagating radially from the edifice axis) as a function of the depth and lateral distance from the axis. Stresses are numerically calculated, solving the equations for linear elasticity with the “Finite Element Method” (COMSOL software). By convention, compressive stresses are taken as positive. (a) Case of reference without any edifice load at the surface. There is no flexure of the crust, and the horizontal stress does not depend on the lateral distance but only increases with depth due to lithostatic load. (b) Case studied with an edifice acting as a load at the surface and inducing a flexure of the crust. At the axis beneath the edifice, due to the crustal flexure, compression is induced in the upper part of the crust and tension in the lower part. This stress acts together with the lithostatic load, such that the horizontal stress is compressive and almost invariant with the depth at the axis. Vertical dashed lines are for the vertical profiles considered in Figure 10 (at 5, 10, 15, and 20 km from the axis).

can see that this phenomenon occurs at a shallower depth at some distance from the edifice center than directly beneath the edifice because the compressive effect of the edifice load in the upper part of the lithosphere decreases when going away from the edifice.

[33] At El Hierro, vertical progression of magma was stopped when it reached the crustal bottom boundary. Considering only the stress field induced by the lithospheric flexure, it should not be the case because the magma should be well overpressurized at the crustal bottom boundary

(see Figure 10). To explain this behavior, we have to consider a local effect as the presence of an intrusive complex characterized by a different rheology. The magma started propagating laterally toward the edifice center, but the eruption only occurred at the opposite flank. This first-order behavior is well explained by the flexural effect. If magma is stacked at the lower lithospheric boundary, it will extend laterally, possibly forming a local sill [Kavanagh *et al.*, 2006]. It will then tend to propagate laterally toward the edifice center because of the stress field generated by the

Table 2. Parameter Values Used for the Numerical Calculation

Geometrical parameters (km)		Physical parameters	
H_edifice	5.5	Crustal density ρ_c (kg/m ³)	2900
R_edifice	29.3	Edifice density ρ_{ed} (kg/m ³)	2800
R_domain	500	Poisson's ratio ν_c	0.25
H_crust	15	Young's modulus E_c (GPa)	30
H_water	4	Gravity g (m/s ²)	9.81
		Mantle density ρ_m (kg/m ³)	3300
		Water density ρ_w (kg/m ³)	1000

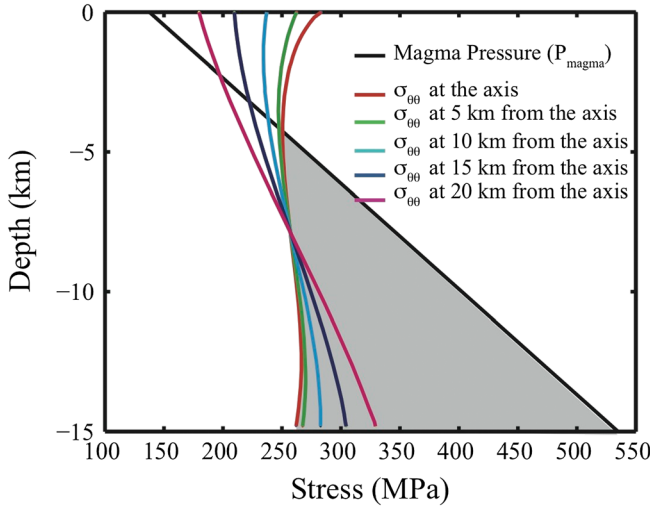


Figure 10. Stress field profiles within the elastic crust at various distances from the axis of symmetry (0, 5, 10, 15, 20 km). By convention, compressive stresses are taken as positive. Colored curves show the stress component $\sigma_{\theta\theta}$, which is the normal stress acting on the wall of a vertical dyke propagating radially toward or away from the edifice. The magma pressure profile within a basanitic dyke rising from a depth of 25 km is also shown (black line). The distance between the black curve and the colored ones corresponds to the elastic overpressure within a static dyke compared to the surrounding field and is directly proportional to its opening. The grey area is for the overpressure within a vertical dyke rising at the axis of symmetry beneath the center of the volcano.

lithospheric flexure. However, magma ascent toward the surface is not expected to occur directly beneath the edifice center due to the compressive effect induced in the upper part of the lithosphere, such that this lateral migration should overshoot the edifice center and result in a vertical ascent at some distance on the edifice flank. The fact that magma migration occurred through a NE fracture zone indicates that the regional/local tectonics also played an important role, which should be taken into consideration in a future three-dimensional model. It is worth noting that the path followed by the El Hierro magma, as well as the orientation of the eruption fissure, defines a stress configuration in which the maximum compressional stress is oriented approximately N-S, and the minimum compressional stress is E-W. A N-S tectonic stress would have prevented the opening of magma fractures oriented E-W (i.e., the western rift zone, see Figure 1) but would have facilitated the opening of structures oriented N-S as it was the eruption fissure.

[34] This simple numerical model only takes into account the flexural effect, and we assume that the stress field induced by this effect should have been constant during the Holocene, as no significant modifications of the morphology of the island have occurred at that time. This could lead us to question why, if the stress field is the same, magma has not followed the same path than previous eruptions. However, having the same stress field does not mean that magma propagation should follow the same path for each eruption, as each path will depend on the initial position of the ascent and on the balance between the driving pressure and the influence of the local stress field [Watanabe *et al.*, 1999]. Also, the tectonic effect should be added to the flexural one. For the effect of the tectonic stress field, dyke opening should occur in the direction of smallest compressive stress, such that an ascent along the southern rift is clearly consistent with a N-S compression. Anyway, a complete model should consider both the flexural effect and the regional tectonic stress field, so it would require a 3D model, but this is beyond the scope of this paper and will be developed elsewhere.

5. Discussion

[35] The comparison of the temporal evolution of the main geophysical and petrological variables and the elaboration of a mechanistic model on magma propagation in the crust allow us to obtain a volcanological model that explains the causes and mechanisms of the El Hierro eruption (Figure 11). This model helps to understand how the eruption was preparing some months before its onset on 10 October 2011 and how it then developed. The model aims to contribute to correctly interpret the geological significance of the precursory signals. This is a key aspect in volcano forecasting, and it will be useful to anticipate future eruptions in the Canary Islands or other areas with similar characteristics.

[36] The evolution of seismicity and surface deformation reveals that magma accumulated for 2 months at the north of the island, at the crust/mantle discontinuity (12–15 km deep), and then migrated SE, maintaining the same depth for nearly 20 km before triggering the eruption. Geophysical and petrological data suggest the existence of two main eruptive episodes marked by different patterns of seismicity, surface deformation, amplitude of the tremor signal, and by significant changes in composition and rheology of the erupted magmas. The main changes observed between the two episodes seem to correspond to stress and rheological changes in the plumbing system induced by decompression during eruption. Unfortunately, the lack of a continuous record of samples of the erupted products impedes to set up a more precise correlation between geophysical and petrological variations, but we consider that the main changes have been identified. Therefore, we may tentatively propose a volcanological model that explains the preparation and development of the El Hierro eruption.

[37] An overpressurized batch of magma, probably coming from a deeper reservoir located at 20–25 km, raised up vertically through an aseismic channel defined by a major structural discontinuity and progressively accumulated for nearly 2 months at the crust/mantle boundary beneath the north of El Hierro, forming a new magma chamber. The absence of deeper seismicity during this period suggests that

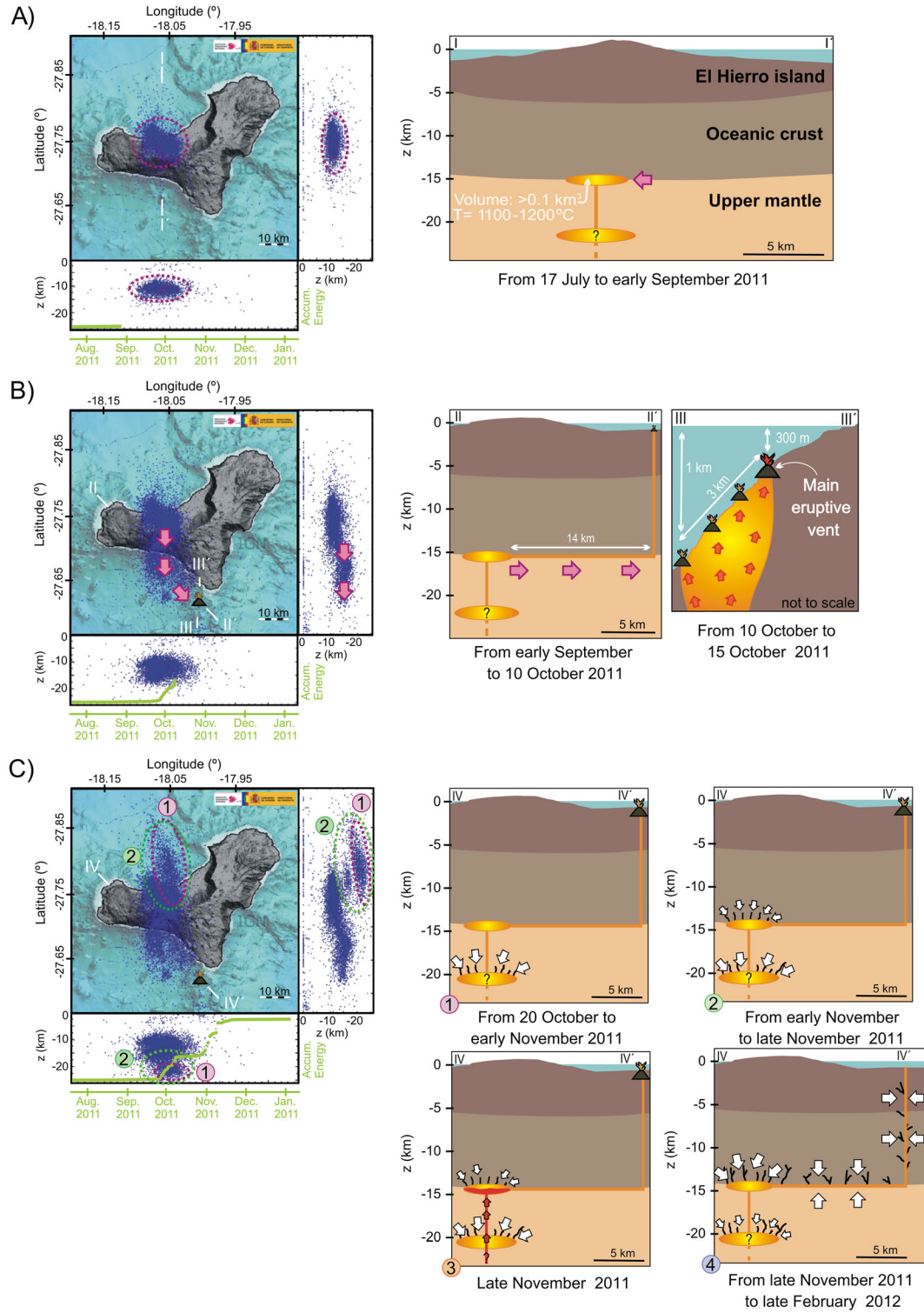


Figure 11. Cartoon representing a volcanological model of the El Hierro eruption. Vignettes at the left show plan views and E-W and N-S distribution of seismicity with time, (a) from 17 July to early September 2011, (b) from early September to 15 October 2011, and (c) from 20 October 2011 to late February 2012. The curve of accumulated seismic energy released for each period is also shown (in green). Vignettes at the right show interpretative cross sections (location is indicated on the left-hand side maps) of the position of magma and state of reservoirs at different times of the process. White arrows indicate compression over different parts of the plumbing system due to its progressive decompression caused by the withdrawal of magma. Intrusion of new magma into the shallow part of the plumbing system occurred on late November 2011 (indicated in red). See text for more explanation.

the internal (over)pressure was maintained in the deeper reservoir during the formation of the new shallower reservoir. This may be explained by new inputs of deeper magma into the deeper reservoir, as seems to be suggested by the petrological data [Martí *et al.*, accepted_b]. The minimum volume of magma intruded at a depth of 10–15 km had to be of the same order with the total erupted volume ($\sim 0.2 \text{ km}^3$) or larger, but it has not been calculated in this study.

[38] The stress field imposed by the flexural effect of the island on the site where magma was accumulating to form the shallower reservoir, together with the prevailing tectonic stress, favored the lateral migration of magma toward the south along the crust/mantle discontinuity, instead of allowing to continue its vertical ascent to the surface. Moreover, this lateral migration was affected by the existence of stress barriers created by rheological contrasts in the lower crust probably due to the presence of high-density bodies that correspond to the roots of previous eruptions. Under this stress configuration, magma could not find a suitable path to reach the surface until it did not meet a N-S-oriented fracture with sufficient low strength to be opened by the driving overpressure of magma, and this occurred when magma reached the southern rift.

[39] During this episode of magma accumulation and migration, magma started to differentiate by fractional crystallization at a depth of 12–15 km in the newly formed magma chamber, which also underwent extensive zonation. When the eruption started, the first magmas to reach the surface were the most differentiated, and progressively, lesser evolved magmas were emitted, thus confirming the existence of zonation in the magma chamber. The timescale at which this differentiation occurred was 3 months, as it is indicated by the duration of the unrest episode and confirmed by the diffusion modeling results, which show that the equilibration of olivine crystals occurred in a time period of 1.5 to 3 months [Martí *et al.*, accepted].

[40] The analysis of seismicity and surface deformation shows how, during the inflation episode preceding the eruption, the oceanic crust deformed elastically, and then it became brittle when the elastic response was exceeded. This deformation clearly accounts for the space that magma needed to accommodate at the base of El Hierro's oceanic crust. Most of the seismicity occurred during this first part of the unrest episode corresponded to magma-driven fracturing, probably caused by a radial expansion of magma when forming the new magma chamber (Figure 5d). However, the seismicity pattern changed significantly when the lateral migration of magma occurred, recording the strongest earthquakes of the whole unrest period. During this episode, seismicity was mostly associated with shear fracturing rather than with magma-driven fracturing (Figure 5d), and this suggests that magma opened its path by pushing away the crust and readjusting previous fractures and faults. Therefore, most of the deformation recorded during the unrest episode was due to the formation and pressurization of the plumbing system due to the arrival of overpressurized magma at shallower levels and its degassing during cooling and crystallization. In fact, anomalous gas (CO_2) emissions were detected during the unrest episode in some places, coinciding with the concentration of seismic events [López *et al.*, 2012], thus not only indicating a massive degassing of magma, but also an increase in the permeability of the host rock induced by fracturing.

[41] The eruption of magma progressively decompressed the plumbing system, which had to re-accommodate to the new stress conditions. During eruption, seismicity was mostly due to shear fracturing and responded to gravitational and tectonic readjustments of the plumbing system. These stress changes marked also the way in which magma was extruded, causing changes in the intensity of the eruption that were also recorded as changes in the intensity of the tremor signal at the vent (Figure 5e). Also, the composition and rheology of the erupting magma was influenced by these stress changes that facilitated the arrival of new inputs of fresher magma at the shallower part of the plumbing system. Once the eruption initiated, the plumbing systems remained overpressurized for some days, after which the lower part started to readjust to the decreasing internal pressure. This was marked by an intense seismicity located at the north of the island at a depth of 20–25 km (Figure 2). A few days later, seismicity also started at a depth of 10–15 km, thus also indicating the readjustment of the upper part of the plumbing system. The readjustment of the deeper part of the plumbing system ended by late November 2011, coinciding with a recharge episode of the shallow magma chamber that was marked by changes in composition and rheology of the erupting magma. After that and until the end of the eruption by late February 2012, most of the seismicity was concentrated at a depth of 10–15 km and not only at the north, but also at the south, along the path that magma followed to reach the eruption site. This suggests that during this second eruptive episode decompression of the plumbing systems mostly affected its uppermost part, with the deeper part playing a passive role. After the eruption, some seismicity has continued in the whole area at depths ranging from 10 to 25 km (www.ign.es), which indicates that the oceanic crust was trying to recover its former state of stress from the perturbation caused by the intrusion of magma at shallower levels. On 24 June 2012, a new strong seismic swarm started and lasted until mid-July, having associated significant surface deformation (www.ign.es). This correlates with a new intrusion of magma below El Hierro, this time at a depth of 20–25 km, and suggests that magmatic activity has not ended yet and that new eruptions might occur in the near future. However, the analysis and interpretation of this possible new intrusion episode is beyond the scope of this paper and is not considered here.

[42] El Hierro eruption has confirmed the results of a probabilistic analysis of having a new basaltic eruption in the Canary Islands, which concluded that the probability for the next 20 years is 99% [Sobradelo *et al.*, 2011]. This probabilistic study also suggested that the highest likelihood of hosting a future eruption corresponded to the islands of Lanzarote, Tenerife, and La Palma, as these were the only ones that show historical volcanism. The fact that El Hierro Island was not considered as a potential location for a new eruption may be due to the incompleteness of historical records which would have biased the results obtained. In fact, Hernández-Pacheco [1982] postulated that an eruption from which no historical records (chronicles) exist could have occurred in 1793 at Lomo Negro, at the western corner of the island, at the same time when a strong seismic swarm was felt by El Hierro inhabitants, which they had registered in their reports. However, there were no direct observations of that eruption, so it was not included in the catalogue of

historical volcanism of the Canary Islands [Romero, 1991] that was used to perform the statistical analysis of *Sobrado et al.* [2011]. Moreover, the fact that this new eruption has been submarine opens the possibility that other submarine eruptions may have occurred in historical times without having been recorded in the historical volcanism catalogue. In fact, several seismic crises apparently not associated with volcanic activity have been reported in the Canarian historical chronicles [Romero, 1991]. Also, bathymetric studies [Romero et al., 2000; Gee et al., 2001; Rivera et al., 2013] show that a large number of well-preserved volcanic cones are present on the submarine flanks of the Canary Islands, so we cannot rule out the possibility of having a larger number of historical eruptions than that corresponding to the sub-aerial ones recorded in the local chronicles. If that was the case, then the recurrence of basaltic volcanism in the Canary Islands would be shorter than suggested by *Sobrado et al.* [2011], so the associated volcanic hazard and risk would be higher.

6. Conclusions

[43] The El Hierro eruption provides a good example on how magma prepares to erupt and how its movement in the upper lithosphere is controlled by the stress field. The driving overpressure of the magma, which is a function of its volume, density, and rheology, determines to which extent magma will move inside the lithosphere and whether or not it will erupt on the surface. However, it does not determine where and when the eruption will occur. These are two key questions we need to answer when monitoring systems detect anomalous activity that could be precursory to an eruption. Determining when and where the eruption will occur does not only depend on the identification of the geophysical and geochemical precursors, but also on their correct interpretation in geological and petrological terms. The El Hierro eruption shows how important stress distribution inside the crust is and how this is influenced by rheological contrasts, existence of tectonic stresses, and gravitational loading (topography). Also, the tectonic structure exerts a significant role in controlling how magma can move and where it can erupt. The coupled interpretation of geophysical and petrological data, combined with stress modeling, made after the eruption has proven to be the correct way to interpret the eruption. Unfortunately, it is too late to forecast that eruption, but this view may help to better forecast and understand future eruptions in the Canary Islands or similar active volcanic areas.

[44] **Acknowledgments.** This research has been supported by IGN and CSIC, and EC grant VUELCO and the MINECO grant CGL2011-16144-E. AG is grateful for her Juan de la Cierva Grant (JCI-2010-06092).

References

Aki, K., and P. G. Richards (1980), *Quantitative Seismology: Theory and Methods*, vol. 1, p. 557, Freeman and Co., San Francisco.

Ancochea, E., et al. (2004), Canarias y el vulcanismo neógeno peninsular, in *Geología de España*, edited by J. A. Vera, pp. 635–682, Instituto Geológico y Minero de España (IGME) y Sociedad Geológica de España (SGE), Madrid.

Anguita, F., and F. Hernan (1975), A propagating fracture model versus a hot spot origin for the Canary islands, *Earth Planet. Sci. Lett.*, 27, 11–19.

Anguita, F., and F. Hernan (2000), The Canary Islands: A unifying model, *J. Volcanol. Geotherm. Res.*, 103, 1–26.

Araña, V., and R. Ortiz (1991), The Canary Islands: Tectonics, magmatism and geodynamic framework, in *Magmatism in Extensional Structural Settings: The Phanerozoic African Plate*, edited by A. B. Kampunzu and R. T. Lubala, pp. 209–249, The Phanerozoic African Plate. Springer-Verlag, Germany.

Bosshard, E., and D. J. MacFarlane (1970), Crustal structure of the western Canary Island from seismic refraction and gravity data, *J. Geophys. Res.*, 75, 4901–4918.

Carbó, A., A., Muñoz-Martín, P. Llanes, J. Alvarez, and EEZ Working Group. (2003), Gravity analysis offshore the Canary Islands from a systematic survey, *Marine Geophys. Res.*, 24, 113–127.

Carracedo, J. C., S. Day, H. Guillou, E. Rodriguez Badiola, J. A. Canas, and F. J. Pérez-Torrado (1998), Hotspot volcanism close to a passive continental margin: the Canary Islands, *Geol. Mag.*, 135, 591–604.

Carracedo, J. C., E. Rodriguez-Badiola, H. Guillou, J. de La Nuez, and F. J. Pérez Torrado (2001), Geology and volcanology of La Palma and El Hierro, Western Canaries, *Estud. Geol.*, 57, 175–273.

Chen, P., and H. Chen (1989), Scaling law and its applications to earthquake statistical relations, *Tectonophysics*, 166, 53–72.

Chouet, B. H. (1996), Long-period volcano seismicity: Its source and use in eruption forecasting, *Nature*, 380, 309–316.

Galgana, G. A., and P. J. McGovern, and E. B. Grosfils (2011), Evolution of large Venusian volcanoes: Insights from coupled models of lithospheric flexure and magma reservoir pressurization, *J. Geophys. Res.*, 116, E03009, doi:10.1029/2010JE003654

Gee, M. J. R., D. G. Masson, A. B. Watts, and N. C. Mitchell (2001), Offshore continuation of volcanic rift zones, El Hierro, Canary Islands, *J. Volcanol. Geotherm. Res.*, 105, 107–119. doi:10.1016/S0377-0273(00)00241-9

Guillou, H., J. C. Carracedo, F. Perez-Torrado, and E. Rodriguez Badiola (1996), K-Ar ages and magnetic stratigraphy of a hotspot-induced, fast grown oceanic island: El Hierro, Canary Islands, *J. Volcanol. Geotherm. Res.*, 73, 141–155.

Gutenberg, B., and C. F. Richter (1954), *Seismicity of the Earth*, 2nd ed., p. 310, Princeton University Press, Princeton, N. J.

Hernandez-Pacheco, A. (1982), Sobre una posible erupción en 1793 en la isla de El Hierro (Canarias), *Estud. Geol.*, 38, 15–25.

Hill D. P., J. O. Langbein, and S. Prejean (2003), Relations between seismicity and deformation during unrest in Long Valley caldera, California, from 1995 through 1999, *J. Volcanol. Geotherm. Res.*, 127, 175–193.

Hoernle, K. A. J., and H.-U. Schmincke (1993), The role of partial melting in the 15-Ma geochemical evolution of Gran Canaria: A blob model for the Canary hotspot, *J. Petrol.*, 34, 599–626.

Hoernle, K., Y. S. Zhang, and D. Graham (1995), Seismic and geochemical evidence for large-scale mantle upwelling beneath the eastern Atlantic and western and central Europe, *Nature*, 374, 34–39, doi:10.1038/374034a0.

Jellinek, A. M., and D. Bercovici (2011), Seismic tremors and magma wagging during explosive volcanism, *Nature*, 470, 522–525.

Kavanagh, J. L., T. Menand, and S. Sparks (2006), An experimental investigation of sill formation and propagation in layered media, 2006, *Earth Planet. Sci. Lett.*, 245, 799–813.

Le Bas, M. J., D. C. Rex, and C. J. Stillman (1986), The early magmatic chronology of Fuerteventura, Canary Islands, *Geol. Mag.*, 123, 287–298.

Le Pichon, X., and P. J. Fox (1971), Marginal offsets, fracture zones, and the early opening of the North Atlantic, *J. Geophys. Res.*, 76, 6294–6308.

Lister, J. R. (1990), Buoyancy-driven fluid fracture: The effects of material toughness and low-viscosity precursors, *J. Fluid Mech.*, 210, 263–280.

Lister, J. R., and R. C. Kerr (1991), Fluid-mechanical models of crack propagation and their application to magma transport in dykes, 1991, *J. Geophys. Res.*, 96, 10,049–10,07.

López, C., et al. (2012), Monitoring the unrest of El Hierro (Canary Islands) before the onset of the 2011 submarine eruption, *Geophys. Res. Lett.*, 39, L13303, doi:10.1029/2012GL051846.

Maccaferri, F., M. Bonafede, and E. Rivalta (2011), A quantitative study of the mechanisms governing dike propagation, dyke arrest and sill formation, 2011, *J. Volcanol. Geotherm. Res.*, 208, 39–50.

Marinoni, L. B., and G. Pasquarè (1994), Tectonic evolution of the emergent part of a volcanic ocean island: Lanzarote, Canary Islands, *Tectonophysics*, 239, 111–135.

Martí, J., R. Ortiz, J. Gottsmann, A. García, and S. De La Cruz-Reyna (2009), Characterising unrest during the reawakening of the central volcanic complex on Tenerife, Canary Islands, 2004–2005, and implications for assessing hazards and risk mitigation, *J. Volcanol. Geotherm. Res.*, 182, 23–33.

Martí, J., A. Castro, C. Rodríguez, F. Costa, S. Carrasquilla, R. Pedreira, and X. Bolos (2013), Correlation of magma evolution and geophysical monitoring at the El Hierro (Canary Islands) 2011–2012 submarine eruption, *J. Petrol.*, accepted.

Matsuki, K. (1991), Three-dimensional in-situ stress measurement with anelastic strain recovery of a rock core, in *Proceedings of the 7th*

- International Congress on Rock Mechanics, edited by W. Wittke, pp. 557–560, Taylor and Francis, London.
- McGovern, P. J., and S. C. Solomon (1993), State of stress, faulting, and eruption characteristics of large volcanoes on Mars, *J. Geophys. Res.*, **98**, 23,553–23,579.
- McNutt, S. R. (2005), Volcano seismology, *Ann. Rev. Earth Planet. Sci.*, **33**, 461–491.
- Montesinos, F. G., J. Amoso, M. Benavent, and R. Vieira (2006), The crustal structure of El Hierro (Canary Islands) from 3-D gravity inversion, *J. Volcanol. Geotherm. Res.*, **150**, 283–299.
- Pedersen, R., and F. Sigmundsson (2006), Temporal development of the 1999 intrusive episode in the Eyjafjallajökull volcano, Iceland, derived from InSAR images, *Bul. Volcanol.*, **68**, 377–393.
- Perez-Torrado, F. J., J. C. Carracedo, A. Rodríguez-Gonzalez, V. Soler, V. R. Troll, and S. Wiesmaier (2012), La erupción submarina de La Restinga en la isla de El Hierro, Canarias: Octubre 2011-Marzo 2012, *Estud. Geol.*, **68**, 5–27, doi:10.3989/egol.40918.179.
- Pettford, N., A. R. Cruden, K. J. W. McCaffrey, and J.-L. Vigneresse (2000), Granite magma formation, transport and emplacement in the Earth's crust, *2000, Nature*, **408**, 669–673.
- Pinel, V., and C. Jaupart (2004), Magma storage and horizontal dyke injection beneath a volcanic edifice, *Earth and Planet. Sci. Lett.*, **221**, 245–262.
- Pinel, V., F. Sigmundsson, E. Sturkell, H. Geirsson, P. Einarsson, M. T. Gudmundsson, and T. Högnadóttir (2007), Discriminating volcano deformation due to magma movements and variable surface loads: Application to Katla subglacial volcano, Iceland, *Geophys. J. Int.*, **169**, 325–338.
- Rivera, J., G. Lastras, M. Canals, J. Acosta, B. Arrese, N. Hermida, A. Micallef, O. Tello, and D. Amblas (2013), Construction of an oceanic island: Insights from the El Hierro (Canary Islands), *Geology*, doi:10.1130/G33863.1.
- Robertson, A. H. F., and C. J. Stillman (1979), Late Mesozoic sedimentary rocks of Fuerteventura, Canary Islands. Implications for West Africa continental margin evolution, *J. Geol. Soc. London*, **136**, 47–60.
- Romero, C. (1991), Las manifestaciones volcánicas históricas del archipiélago canario, Consejería de Política Territorial, Gobierno Autónomo de Canarias, 2 tomos, Santa Cruz de Tenerife.
- Romero, C., L. Garcá-Cacho, V. Araña, A. Yanes-Luque, and A. Felpeto (2000), Submarine volcanism surrounding Tenerife, Canary Islands: Implications for tectonic controls, and oceanic shield forming processes, *J. Volcanol. Geotherm. Res.*, **103**, 105–119.
- Rubin, A. M. (1993), Dikes versus diapirs in viscoelastic rock, *Earth Planet. Sci. Lett.*, **117**, 653–670.
- Schmincke, H.-U. (1982), Volcanic and geochemical evolution of the Canary Islands, in *Geology of the Northwest African Continental Margin*, edited by U. von Rad, K. Hinz, M. Sarnthein and E. Siebold, pp. 273–306, Springer-Verlag, Berlin.
- Sigmarrsson, O., D. Laporte, B. Devouard, J. Martí, J. L. Devidal, and M. Carpentier (2012), Formation of U-depleted rhyolite from a basanite at El Hierro, Canary Islands, *Contrib. Mineral. Petrol.*, doi:10.1007/s00410-012-0826-5.
- Sigmundsson, F., et al. (2010), Intrusion triggering of the 2010 Eyjafjallajökull explosive eruption, *Nature*, **468**, 426–432.
- Sobradelo, R., J. Martí, A. T. Mendoza-Rosas, and G. Gómez (2011), Volcanic hazard assessment for the Canary Islands (Spain) using extreme value theory, *Nat. Haz. Earth Sys. Sci.*, **11**, 2741–2753.
- Stronck, N. A., A. Klügel, and T. H. Hansteen (2009), The magmatic plumbing system beneath El Hierro (Canary Islands): Constraints from phenocrysts and naturally quenched basaltic glasses in submarine rocks, *Contrib. Mineral. Petrol.*, **157**, 593–607.
- Tarasiewicz, J., R. S. White, A. W. Woods, B. Brandsdóttir, and M. T. Gudmundsson (2012), Magma mobilization by downward-propagating decompression of the Eyjafjallajökull volcanic plumbing system, *Geophys. Res. Lett.*, **39**, L19309, doi:10.1029/2012GL053518.
- Traversa, P., V. Pinel, and J.-R. Grasso (2010), A constant influx model for dike propagation: Implications for magma reservoir dynamics, *J. Geophys. Res.*, **115**, B01201, doi:10.1029/2009JB006559.
- Troll, V. R., et al. (2011), Floating sandstones off El Hierro (Canary Islands, Spain): The peculiar case of the October 2011 eruption, *Solid Earth Discuss.*, **3**, 975–999, www.solid-earth-discuss.net/3/975/2011/, doi:10.5194/se-3-975-2011.
- Voight, B. (1968), Determination of the virgin state of stress in the vicinity of a borehole from measurements of a partial anelastic strain tensor in drill cores, *Felsmech. Ingenieurgeol.*, **6**, 201–215.
- Watanabe, T., T. Koyaguchi, and T. Seno (1999), Tectonic stress controls on ascent and emplacement of magmas, *J. Volcanol. Geotherm. Res.*, **91**, 65–78.
- Watts, A. B. (1994), Crustal structure, gravity anomalies and flexure of lithosphere in the vicinity of the Canary Islands, *Geophys. J. Intern.*, **119**, 648–666.
- Watts, A. B., C. Peirce, J. Collier, R. Dalwood, J. P. Canales, and T. J. Henstock (1997), A seismic study of lithospheric flexure in the vicinity of Tenerife, Canary Islands, *Earth Planet. Sci. Lett.*, **146**, 431–447.
- Yokoyama, I. (1988), Seismic energy releases from volcanoes, *Bull. Volcanol.*, **50**, 1–13.